Nonthermal distributions of charmed hadrons in relativistic heavy-ion collisions

Chaoyu Pan, Shuhan Zheng, Meimei Yang, Zhiwei Liu, and Baoyi Chen*
Department of Physics, Tianjin University, Tianjin 300354, China

(Received 24 March 2023; revised 24 June 2023; accepted 22 August 2023; published 5 September 2023)

We employ the Boltzmann transport model to study the charmonium regeneration with nonthermal charm quarks in relativistic heavy-ion collisions. As heavy quarks do not reach kinetic thermalization in the quark-gluon plasma (QGP), the final transverse momentum distribution of regenerated charmonium depends on the degree of charm quark kinetic thermalization. When the charm momentum distribution becomes harder, more charm quarks are distributed in the middle ($3 < p_T < 6$ GeV/c) and high ($p_T \geqslant 6$ GeV/c) p_T, where the production of regenerated charmonium also becomes larger. In this work, we explore the degree of charm quark kinetic thermalization qualitatively and its effect on the charmonium distribution. With nonthermal momentum distribution of charm quarks in the coalescence process, the nuclear modification factor $R_{AA}(p_T)$ of charmonium enhances at middle p_T. Besides, the elliptic flow $v_2(p_T)$ of charmonium also enhances at middle p_T as more regenerated charmonium are distributed in this p_T region. The theoretical calculations with nonthermal charm distribution explain well the p_T dependence of charmonium R_{AA} and v_2, which indicates that charm quarks do not reach complete kinetic thermalization in the QGP when charmonium are regenerated.

DOI: 10.1103/PhysRevC.108.034903

I. INTRODUCTION

In relativistic heavy-ion collisions, it is believed that an extremely hot and deconfined medium made up of quarks and gluons, called "quark-gluon plasma" (QGP) is produced [1]. The study of signals [2,3] and properties [4] of this new deconfined matter, such as transport coefficients and initial energy densities helps to comprehend the strong interaction at finite temperatures. Heavy quarks and quarkonium are predominantly produced in the nuclear parton hard scatterings due to their large masses. They have been proposed as clean probes of early stage of the hot medium generated in nucleus-nucleus (AA) collisions in the CERN Large Hadron Collider (LHC) and the BNL Relativistic Heavy Ion Collider (RHIC) [5–10]. In this hot medium, the heavy quark potential is screened by thermal light partons [11,12], which results in the "melt" of quarkonium-bound states when the medium temperature is sufficiently high [13,14]. The highest temperature at which quarkonium-bound states can survive is called the "dissociation temperature" T_d [15–17]. Below this T_d, inelastic collisions from thermal light partons can also dissociate the quarkonium-bound states [18–20]. The survival probability of quarkonium decreases when traveling through the QGP due to both color screening and parton inelastic scatterings. The hot medium effects are characterized by the nuclear modification factor R_{AA}, which is defined as the ratio of quarkonium production in AA collisions to the production in proton-proton (pp) collisions scaled by the number of nucleon binary collisions $N_{\rm coll}$.

At the LHC, where there are many heavy quarks in the QGP, charm and anticharm quarks have a significant chance to combine into new bound states above the critical temperature $T_c \approx 165$ MeV above which charm flavor exists as charm quarks instead of D mesons. This process becomes even more dominant in the production of charmonium with the presence of more charm pairs [21,22]. As charm quarks lose energy as they travel through the QGP [23–31], the final p_T spectrum of charm quarks and the regenerated charmonium from the coalescence process differs with the coupling strength between charm quarks and the medium. Experimental observables such as the collective flows of D mesons suggest that the final distributions of D mesons are close to kinetic thermalization [32,33]. However, it is still undetermined whether charm quarks have achieved kinetic thermalization in the hypersurface of charmonium regeneration at $T > T_c$. The process of charm quark energy loss in the hot medium has been extensively studied using Langevin equations [7,34,35] and transport equations [36,37]. The momentum distribution of regenerated charmonium varies depending on the degree of charm quark kinetic thermalization, which can alter the shape of the charmonium nuclear modification factor and elliptic flows [38–40]. In the scenario where charm quarks have fully achieved kinetic thermalization [8], most regenerated charmonium are distributed at low p_T. When charm quarks experience less energy loss in the medium, the regenerated charmonium tends to carry higher momentum, resulting in an increase in R_{AA} at the middle p_T region. This may also shift the peak of $v_2(p_T)$ to the higher p_T region.

This work studies the p_T dependence of charmonium $R_{AA}(p_T)$ and $v_2(p_T)$ by employing various momentum distributions of charm quarks. Cold nuclear matter effects have been included in the initial distributions of charm quarks and

*baoyi.chen@tju.edu.cn

charmonium [41–43]. Hot medium evolution is described using hydrodynamic equations [44–46]. The paper is organized as follows. In Sec. II, the transport model is introduced. In Sec. III, nonthermal distributions of charm quarks are discussed. Hot medium evolution is given as a background in Sec. IV. In Sec. V, the initial conditions of charmonium are introduced. The scaled R_{AA} and v_2 of charmonium are then calculated and compared with experimental data for different nonthermal momentum distributions of charm quarks in Sec. VI. Lastly, a final summary is given in Sec. VII.

II. TRANSPORT MODEL

The distribution of heavy quarkonium in a medium has been extensively studied using various models, including transport models [47–51], coalescence models [22,52,53], statistical hadronization model [54], open quantum system approaches [55–61], etc. The transport model takes into account both primordial production and regeneration. The Boltzmann transport equation for charmonium evolution is written as [8]

$$\partial_t f_\psi + \mathbf{v}\cdot\nabla_{\mathbf{x}} f_\psi = -\alpha f_\psi + \beta, \tag{1}$$

where the distribution of charmonium in phase space, denoted by f_ψ, varies over time due to charmonium diffusion which is represented by the term $\mathbf{v}\cdot\nabla_{\mathbf{x}} f_\psi$. $\mathbf{v}$ is the velocity of charmonium. ψ here represents three states $\psi = (J/\psi, \chi_c, \psi')$. The decay rate α accounts for inelastic collisions and the color screening effect that can dissociate charmonium states. This rate depends on both the density of light partons and the inelastic cross sections [20],

$$\alpha(\boldsymbol{p}, x) = \frac{1}{2E_T}\int \frac{d^3\boldsymbol{p}_g}{(2\pi)^3 2E_g} W_{g\psi}^{c\bar{c}}(s) f_g(\boldsymbol{p}_g, x)\Theta(T(x) - T_c), \tag{2}$$

where $\mathbf{p}_g$ and E_g are the momentum and the energy of thermal gluons. $E_T = \sqrt{m_\psi^2 + p_T^2}$ is the transverse energy of charmonium with the mass $m_{J/\psi} = 3.1$ GeV. f_g is the Bose distribution of massless gluons. The step function $\Theta(T - T_c)$ ensures that the gluon-dissociation process only happens above the critical temperature T_c of the deconfined phase transition. $W_{g\psi}^{c\bar{c}} = 4\sigma_{g\psi}^{c\bar{c}}(s) F_{g\psi}(s)$ is the charmonium dissociation probability in the reaction $g + J/\psi \to c + \bar{c}$, where s is the center-of-mass energy of the gluon and the charmonium. $F_{g\psi}$ is the flux factor [20]. $\sigma_{g\psi}^{c\bar{c}}$ is the gluon-dissociation cross section. It is obtained via the operator-production-expansion (OPE) method [62,63]

$$\sigma_{g-J/\psi}(\omega) = A_0 \frac{(x-1)^{3/2}}{x^5}. \tag{3}$$

We use w to represent the gluon energy, while x refers to the ratio of the gluon energy to the J/ψ in-medium binding energy ϵ_ψ. The constant factor $A_0 = 2^{11}\pi/(27\sqrt{m_c^3\epsilon_\psi})$ has charm quark mass $m_c = 1.87$ GeV. For the prompt J/ψ in pp collisions, it consists of direct J/ψ and also decays from (χ_c, ψ') states with the fraction of $(60\%, 30\%, 10\%)$ [43], i.e., 10% of prompt J/ψ comes from the decay of ψ'. With these fractions, one can extract the ratio of direct production concerning $(J/\psi, \chi_c, \psi')$ at the beginning of the transport equation. The dynamical evolutions of charmonium excited states exhibit similarities to the ground state, as described by Eq. (1), with updated decay rates derived from the geometric scale [64].

Above the critical temperature, heavy quark potential is partially restored [65,66], allowing charm and anticharm quarks to combine and form new bound states through the reaction $c + \bar{c} \to J/\psi + g$. The regeneration rate of charmonium β is proportional to the densities of charm and anticharm quarks,

$$\begin{aligned}\beta(\boldsymbol{p}, x) = \frac{1}{2E_T}\int &\frac{d^3\boldsymbol{p}_g}{(2\pi)^3 2E_g}\frac{d^3\boldsymbol{p}_c}{(2\pi)^3 2E_c}\frac{d^3\boldsymbol{p}_{\bar{c}}}{(2\pi)^3 2E_{\bar{c}}} \\ &\times W_{c\bar{c}}^{g\psi}(s) f_c(\boldsymbol{p}_c, \mathbf{x}) f_{\bar{c}}(\boldsymbol{p}_{\bar{c}}, \mathbf{x}) \\ &\Theta(T(\mathbf{x}) - T_c)(2\pi)^4\delta(p + p_g - p_c - p_{\bar{c}}),\end{aligned} \tag{4}$$

where $\mathbf{p}_c$ and $\mathbf{p}_{\bar{c}}$ represent the momentum of charm and anticharm quarks, respectively. $E_c = \sqrt{m_c^2 + p_c^2}$ denotes the energy of charm quark. The probability of a combination of c and $\bar{c}$, denoted by $W_{c\bar{c}}^{g\psi}$, is determined through the detailed balance [20]. The δ function $\delta(p + p_g - p_c - p_{\bar{c}})$ ensures a four energy-momentum conservation in the reaction. Charm quark distribution $f_c(\mathbf{p}_c, \mathbf{x})$ in the QGP will be obtained by fitting the results from the Langevin model [67–69].

III. NONTHERMAL DISTRIBUTION OF CHARM QUARKS

Heavy quarks experience significant energy loss when they move through a hot medium. The Langevin equation can be used to obtain the spatial and momentum distributions of heavy quarks. We employ the Langevin model introduced in the previous Ref. [53] to calculate the charm nonthermal distribution. For simplicity, we assume that the heavy quark distribution in phase space can be separated into a product of the spatial density $\rho_c(\mathbf{x}, t)$ and the momentum distribution as $f_c(\mathbf{p}_c, \mathbf{x}, t) = \rho_c(\mathbf{x}, t) f(\mathbf{p}_c, t)$. The spatial density $\rho_c(\mathbf{x}, t)$ decreases with the times in the expanding QGP. It mainly affects the yield of regenerated charmonium. Therefore, we approximate the spatial density with the diffusion equation, $\partial_\mu(\rho_c u^\mu) = 0$ [43], which is usually used in the limit of the kinetic thermalization. The heavy quark spatial density only depends on the four-velocity of the medium, which is given by hydrodynamic equations. The initial profile of ρ_c is proportional to the $d\sigma_{pp}^{c\bar{c}}/dy T_A(x_T - b/2)T_B(x_T + b/2)$, where $d\sigma_{pp}^{c\bar{c}}/dy = (1.165,\ 0.718)$ mb [70,71] are the rapidity differential cross sections of charm quarks in central and forward rapidities, respectively. $T_{A(B)}$ is the nuclear thickness function. The transverse coordinate, x_T, refers to the spatial position in the plane perpendicular to the longitudinal direction, while z corresponds to the longitudinal direction defined as the direction of nuclear acceleration. The impact parameter, denoted by b, is defined as the distance between the trajectories of two nuclear centers.

As for the momentum distribution, charm quarks do not reach kinetic thermalization during charmonium regeneration [39,40]. The realistic momentum distribution of charm quarks in the QGP is obtained by the event-by-event simulations of the Langevin equation [35,72]. Charm quarks are

randomly regenerated according to the momentum distribution obtained from FONLL calculation [73,74]. These charm quarks are evolved in QGP, suffering parton elastic collisions and medium-induced gluon radiation [53]. The spatial diffusion coefficient is taken as $\mathcal{D}_s(2\pi T) = 5$, which has been previously used for open heavy flavor hadrons [75,76]. When charm quarks move to regions with a relatively low temperature, the heavy quark potential is partially restored and c and $\bar{c}$ can combine into a bound state. Most J/ψ are regenerated below the temperature $T_{\rm rege} \approx 1.2\ T_c$ where the heavy quark potential is mostly restored at the distance of the J/ψ radius [14,64]. The normalized momentum distribution of charm quarks on the hypersurface with $T(\mathbf{x}) = T_{\rm rege}$ is given by the Langevin equation at cent. 0–10 % and cent. 20–40 %, according to Refs. [53,77], where cent. refers to centrality. They are plotted as dots in Fig. 1.

To incorporate the nonthermal distribution of charm quarks into the transport model, we use the Fermi distribution to simulate a distribution that is close to the realistic distribution given by the Langevin model,

$$f_c(\mathbf{p}_c) = \frac{N_{\rm norm}}{e^{u\cdot p_c/T_{\rm eff}} + 1}, \tag{5}$$

where u and p_c are the four-velocity and four-momentum of the fluid and charm quarks, respectively. $T_{\rm eff}$ does not represent the temperature of the medium anymore. It characterizes the realistic momentum distribution of charm quarks in the regeneration process and is connected with the degree of charm energy loss in the medium. When charm quarks lose more energy in the hot medium, their momentum distribution becomes softer. In the limit of kinetic thermalization, charm momentum distribution satisfies the normalized Fermi-distribution with $T_{\rm eff}$ taken as the medium temperature. In the nonthermal case, we fit $T_{\rm eff}$ according to the Langevin results (see Fig. 1) to give a harder momentum distribution of charm quarks. $N_{\rm norm}$ is the normalization factor satisfying the relation $\int d\mathbf{p}_c f_c(\mathbf{p}_c) = 1$. We take the spatial diffusion coefficient $\mathcal{D}_s(2\pi T) = 5$ to evolve charm quarks in the QGP and stop the evolution at $T(\mathbf{x}) = T_{\rm rege}$, where charmonium regeneration happens. In Fig. 1, the normalized final transverse momentum distributions of charm quarks in the Pb-Pb collisions with cent. 0–10 % and cent. 20–40 % are plotted with dots. Different distributions are plotted where $T_{\rm eff}$ is taken as different values. In the thermalization limit, $T_{\rm eff}$ is around the medium temperature $1.2T_c \approx 0.198$ MeV, where regeneration happens. When $T_{\rm eff}$ is larger than the medium temperature $T_{\rm rege}$, it indicates that charm quark momentum distribution becomes harder. The line with $T_{\rm eff} \approx 0.4$ GeV fits the Langevin results better than other lines in the cent. 0–10 %. But in cent. 20–40 %, the line with $T_{\rm eff} = 0.5$ GeV fits the Langevin data well. That means the degree of charm kinetic thermalization differs in different collision centralities. We will take different values of $T_{\rm eff}$ in the charmonium regeneration to study the effect of charm nonthermal distributions.

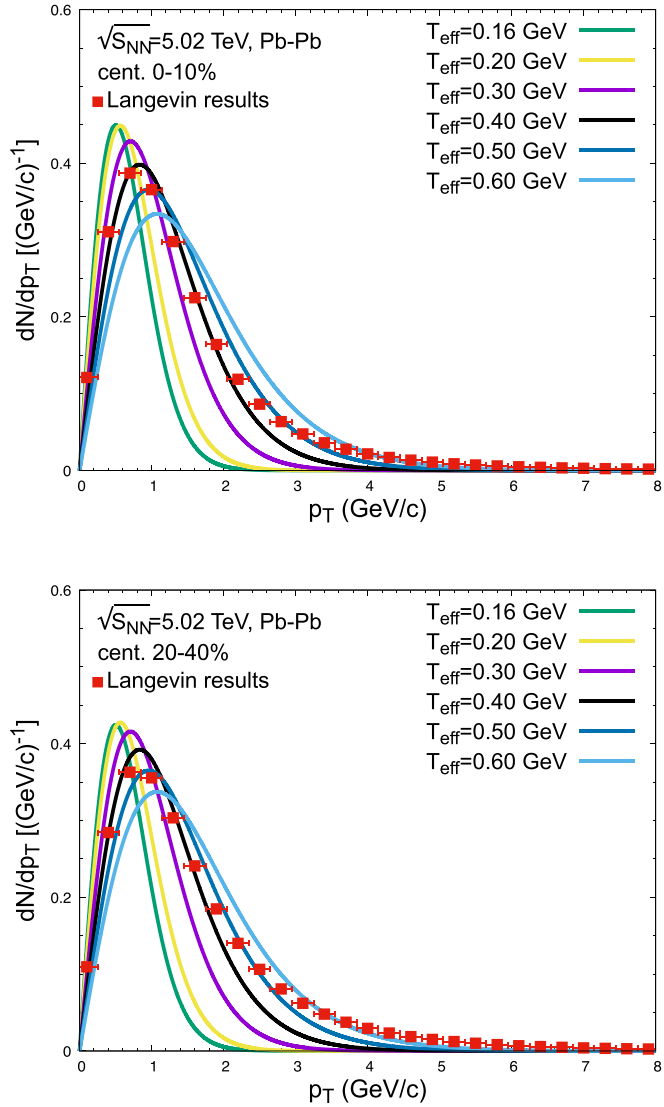

FIG. 1. Upper panel: Normalized transverse momentum distribution dN/dp_T of charm quarks in the cent. 0–10 % of Pb-Pb collisions at $\sqrt{s_{NN}} = 5.02$ TeV. Red squares are the normalized p_T distribution of charm quarks given by the Langevin equation on the hypersurface specified with the J/ψ regeneration temperature $T_{\rm rege}(\mathbf{x}) \approx 1.2\ T_c$. The spatial diffusion coefficient is taken to be $\mathcal{D}_s(2\pi T) = 5$. Different Fermi distributions are plotted where $T_{\rm eff}$ controls the charm quark momentum distribution. Lower panel: Same as the upper panel but with cent. 20–40 %.

IV. HOT MEDIUM EVOLUTION

Relativistic heavy ion collisions produce a hot, deconfined medium that behaves like a nearly perfect fluid. The dynamical evolution of the medium can be described with hydrodynamic equations. We assume that the longitudinal expansion of the hot medium follows a Bjorken evolution and use $2+1$ dimensional ideal hydrodynamic equations to simulate its expansion:

$$\partial_{\mu\nu} T^{\mu\nu} = 0. \tag{6}$$

The energy-momentum tensor is $T^{\mu\nu} = (e+p)u^\mu u^\nu - g^{\mu\nu} p$. u^μ is the four-velocity of the medium. Energy density e and the pressure p change with time and the position. An equation of the state of the medium is necessary to close the equations. QGP is treated as an ideal gas made

up of massless u, d quarks, gluons, and the strange quark with a mass of $m_s = 150$ MeV. Meanwhile the hadronic medium is treated as an ideal gas composed of all known hadrons and resonances with mass up to 2 GeV [78]. The phase transition between the QGP and the hadronic gas is a first-order phase transition with a critical temperature $T_c = 165$ MeV [79]. The initial energy density of the medium is determined by the final charged multiplicity, where the maximum initial temperature at the center of the fireball is extracted to be $T_0(\tau_0, x_T = 0|b = 0) = 510$ MeV at the starting time of hydrodynamic equations in the most central 5.02 TeV Pb-Pb collisions [80]. $\tau_0 = 0.6$ fm is the time scale of the medium reaching local equilibrium [81]. The initial temperatures at other positions x_T are obtained with the Glauber model.

V. INITIAL CONDITIONS

At the beginning of nuclear collisions, charmonium is produced in parton hard scatterings. Their production can be treated as the production in pp collisions scaled with the number of binary collisions $N_{\rm coll}$. In pp collisions without hot medium effects, the momentum distribution of J/ψ has been measured in experiments, which can be parametrized using a power law function [43,82],

$$\frac{d^2\sigma_{pp}^{J/\psi}}{dy 2\pi p_T dp_T} = \frac{(n-1)}{\pi(n-2)\langle p_T^2\rangle_{pp}}\left[1+\frac{p_T^2}{(n-2)\langle p_T^2\rangle_{pp}}\right]^{-n}\frac{d\sigma_{pp}^{J/\psi}}{dy}, \quad (7)$$

where the parameters are fitted to be $\langle p_T^2\rangle_{pp} = 12.5\ (\mathrm{GeV}/c)^2$ and $n = 3.2$ in the central rapidities, and the rapidity differential cross section of inclusive J/ψ is taken to be $d\sigma_{pp}^{J/\psi}/dy = 5.2$ μb (in central rapidity) [82–84]. In the forward rapidity, the differential cross section is fitted to be $d\sigma_{pp}^{J/\psi}/dy = 3.25$ μb. For excited states of charmonium, their normalized p_T distribution is the same as the distribution of J/ψ due to the small difference between their masses. The inclusive charmonium consists of both the nonprompt part from B decay, and the prompt part which is defined as the sum of the primordial production and the regeneration. The inclusive nuclear modification factor related to the prompt and the non-prompt R_{AA} is as follows [17]:

$$R_{AA}^{\rm incl} = \frac{R_{AA}^{\rm prompt}}{1+r_B} + \frac{R_{AA}^{B} r_B}{1+r_B}, \quad (8)$$

where the $R_{AA}^{\rm prompt}$ and R_{AA}^{B} is the prompt and the nonprompt nuclear modification factors. $r_B = f_B/(1-f_B)$ is the ratio of nonprompt and prompt charmonium production in pp collisions. The fraction of nonprompt J/ψ in the inclusive production is fitted to be $f_B = 0.04 + 0.23(p_T/(\mathrm{GeV}/c))$ [84–86], without clear dependence on the collision energy. $R_{AA}^{\rm prompt}$ is calculated with the transport model which includes charmonium dissociation and regeneration. While in the nonprompt part, the final distribution of nonprompt J/ψ is connected with the bottom quark energy loss in the hot medium. The nonprompt nuclear modification factor R_{AA}^{B} can be extracted from the Langevin equation [77].

Charmonium initial distribution in AA collisions is also modified by the cold nuclear matter effects compared with the case in pp collisions. The partons scatter with other nucleons to obtain extra energy before fusing into charm pairs and charmonium. This process is called the Cronin effect [87], making the momentum distribution of primordial charmonium become harder than the distribution extracted in pp collisions. This is included via the modification $\langle p_T^2\rangle_{pp} + a_{gN}\langle l\rangle$. Here, $\langle l\rangle$ is the average path length of partons traveling through the nucleus before the hard scattering. The transverse momentum square parton obtained per unit length is denoted by a_{gN}. The value of a_{gN} is determined to be $a_{gN} = 0.15\ (\mathrm{GeV}/c)^2$ [43,49] based on the charmonium momentum broadening observed in proton-nucleus collisions. Another important cold nuclear matter effect is the shadowing effect [41]. Parton densities in the nucleons of the nucleus become different compared to those in free nucleons. This effect results in the suppression of parton density and hence the reduction of the number of charmonium and charm pairs in heavy-ion collisions. The shadowing effect is calculated to be 0.6 in the most central Pb-Pb collisions at $\sqrt{s_{NN}} = 5.02$ TeV with the EPS09 package [42]. The shadowing factor at other centralities can be obtained via the scale of the thickness function [43].

VI. CHARMONIUM DISTRIBUTION IN HEAVY-ION COLLISIONS

In the regeneration, when the charm quark momentum distribution becomes different, the p_T distribution of regenerated charmonium from the reaction $c + \bar{c} \to J/\psi + g$ also becomes different. Additionally, the total production of charmonium depends on the degree of charm kinetic thermalization. To focus on the shape of charmonium p_T distribution with different nonthermal distributions of charm quarks, the total yields of regeneration are scaled to the same value to fit the experimental data of $R_{AA}(N_p)$ in the most central collisions. With this disposure, we can clearly see how the p_T distribution of charmonium $R_{AA}(p_T)$ and $v_2(p_T)$ are affected by the nonthermal charm quarks, especially at middle and high p_T.

In Fig. 2, we calculated the J/ψ nuclear modification factor as a function of p_T in the centrality 0–10 % in $\sqrt{s_{NN}} = 5.02$ TeV Pb-Pb collisions, where regeneration dominates the total production of J/ψ [64]. With smaller $T_{\rm eff}$, charm quark momentum distribution before regeneration becomes softer (see the lines labeled with $T_{\rm eff} = 0.16, 0.2$ GeV in Fig. 1), leading to regenerated charmonia carry small p_T and are distributed in low p_T region at around $p_T \lesssim 3$ GeV/c. At middle (3–6 GeV/c) and high p_T, regeneration contribution becomes negligible as the density of charm quarks is small, shown as the lines labeled with $T_{\rm eff} = 0.2$ and 0.16 GeV. These lines with softer charm distributions (see green and yellow lines in Fig. 1) underestimate the experimental data at middle p_T. When the momentum distribution of charm quarks becomes harder, such as the cases with $T_{\rm eff} = (0.3, 0.4)$ GeV in Fig. 1, regenerated J/ψ tends to carry larger p_T and enhance the inclusive production of J/ψ at $p_T \approx 4$–5 GeV/c, shown as the lines $T_{\rm eff} = (0.3, 0.4)$ GeV in Fig. 2. However, when the charm momentum distribution used in the regeneration be-

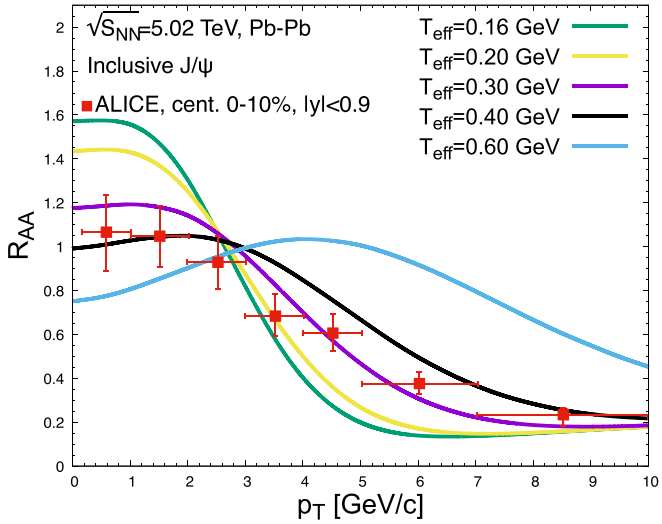

FIG. 2. p_T dependence of inclusive J/ψ nuclear modification factor in the central rapidity of $\sqrt{s_{NN}} = 5.02$ TeV Pb-Pb collisions. Different nonthermal distributions of charm quarks are considered by taking $T_{\rm eff} = (0.16, 0.2, 0.3, 0.4, 0.5, 0.6)$ GeV in the collision centrality 0–10 % where regeneration contribution becomes dominant. The primordial production, regeneration, and decay from B hadron have been included in the lines. The experimental data are cited from the ALICE Collaboration [88].

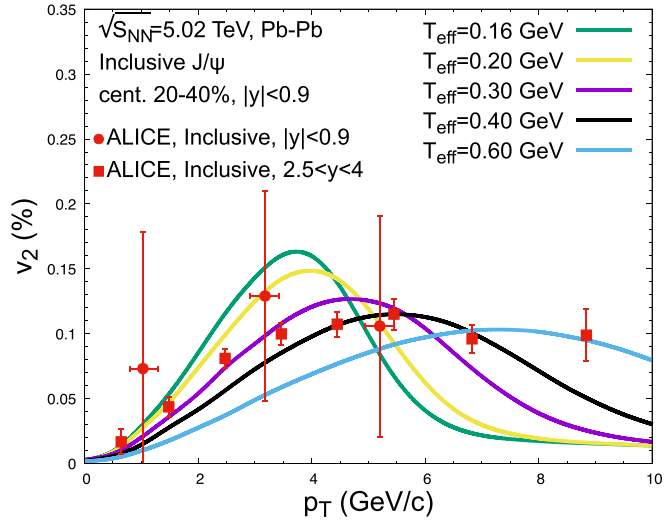

FIG. 3. p_T dependence of inclusive J/ψ elliptic flows in the forward rapidity of $\sqrt{s_{NN}} = 5.02$ TeV Pb-Pb collisions. Different nonthermal distributions of charm quarks are considered by taking $T_{\rm eff} = (0.16, 0.2, 0.3, 0.4, 0.5, 0.6)$ GeV. The experimental data are cited from ALICE Collaboration [89,90].

comes extremely hard ($T_{\rm eff} = 0.6$ GeV), the J/ψ inclusive R_{AA} enhances significantly at high p_T which is far away from the realistic case. Inspired by the realistic distributions of charm quarks given by the Langevin equation in Fig. 1, the value of $T_{\rm eff}$ is expected to be around $T_{\rm eff} \approx 0.4$ GeV. We can see that the shape of the line with $T_{\rm eff} = 0.3$–0.4 GeV can give a better explanation of the data compared to the case of completely kinetic thermalization ($T_{\rm eff} = 0.16$–0.2 GeV).

In Fig. 3, the elliptic flows of inclusive J/ψ are also calculated by taking different nonthermal distributions of charm quarks. Primordially produced charmonium carries small elliptic flows when moving along different trajectories in the anisotropic medium. Charmonium dissociation along different paths results in a nonzero v_2 through medium dissociation. This effect becomes important at large p_T where primordial production dominates the total yield of J/ψ. On the other hand, charm quarks are strongly coupled with QGP. Charm quarks develop collective flows via elastic scatterings with thermal partons, which will be inherited by the regenerated J/ψ. Therefore, when the charm momentum distribution becomes harder such as the lines with $T_{\rm eff} = 0.4$ or 0.6 GeV in Fig. 1, the regenerated J/ψs are mainly distributed at higher p_T. The elliptic flows of inclusive J/ψ are enhanced by the regeneration. When charm quarks are kinetically thermalized, they satisfy a normalized Fermi distribution with the medium temperature $T_{\rm rege}$. In the nonthermal cases, charm distributions become hard, and are characterized by a parameter $T_{\rm eff}$ which is usually larger than the medium temperature. Lines with $T_{\rm eff} \approx 0.4$ GeV can better explain the large v_2 around $p_T \approx 6$ GeV/c than cases with softer charm distributions. This indicates that regeneration is still important in this middle p_T region.

From the shapes of $R_{AA}(p_T)$ and $v_2(p_T)$, one can see that regeneration with nonthermal momentum distributions of charm quarks becomes more important at middle and high p_T. This will increase the elliptic flows of J/ψ at $p_T \approx 6$ GeV/c. While in the thermal case, the contribution of regeneration decreases rapidly with increasing p_T. The parameter $T_{\rm eff}$ characterizing the degree of charm kinetic thermalization is extracted to be around $T_{\rm eff} = 0.3$–0.4 GeV, which is larger than the medium temperatures of charmonium regeneration. Charm momentum distribution is expected to be nonthermal when charmonium regeneration happens, even when D mesons are close to kinetic thermalization after experiencing the whole evolution of the hot medium.

VII. SUMMARY

We employ the transport model to study the p_T distribution of charmonium with nonthermal charm quarks in $\sqrt{s_{NN}} = 5.02$ TeV Pb-Pb collisions. As the heavy quark potential is partially restored above the critical temperature T_c, charmonium can be regenerated above T_c where charm quarks do not reach complete kinetic thermalization. The realistic momentum distribution of charm quarks in charmonium regeneration is simulated with the Langevin equation. To incorporate nonthermal charm distributions into the transport model, we introduce a parameter $T_{\rm eff}$ in a normalized Fermi distribution, where $T_{\rm eff}$ is determined by fitting the realistic distribution of charm quarks from the Langevin model. The value of $T_{\rm eff}$ is found to be larger than the temperature of J/ψ regeneration, which indicates that the charm quark distribution is harder than that in the thermal case. We take different values of $T_{\rm eff}$ in the transport model to calculate $R_{AA}(p_T)$ and $v_2(p_T)$. The regeneration of charmonium with different nonthermal distributions has been scaled to fit the $R_{AA}(N_p)$ of J/ψ, which allows us to focus on the shapes of $R_{AA}(p_T)$ and $v_2(p_T)$ when taking different momentum distributions of charm quarks. The

R_{AA} and v_2 enhance evidently at middle p_T when taking a nonthermal charm distribution, as more charm quarks and regenerated charmonium are distributed in middle and high p_T region. This helps to extract the realistic momentum distribution of charm quarks in charmonium regeneration.

ACKNOWLEDGMENTS

This work is supported by the National Natural Science Foundation of China (NSFC) under Grant No. 12175165.

C.P. and S.Z. contributed equally to this work.

[1] A. Bazavov, T. Bhattacharya, M. Cheng, C. DeTar, H. T. Ding, S. Gottlieb, R. Gupta, P. Hegde, U. M. Heller, F. Karsch *et al.*, Phys. Rev. D **85**, 054503 (2012).
[2] T. Matsui and H. Satz, Phys. Lett. B **178**, 416 (1986).
[3] H. Stoecker, Nucl. Phys. A **750**, 121 (2005).
[4] H. T. Ding, F. Karsch, and S. Mukherjee, Int. J. Mod. Phys. E **24**, 1530007 (2015).
[5] J. Zhao, K. Zhou, S. Chen, and P. Zhuang, Prog. Part. Nucl. Phys. **114**, 103801 (2020).
[6] X. Zhao and R. Rapp, Nucl. Phys. A **859**, 114 (2011).
[7] M. He, R. J. Fries, and R. Rapp, Phys. Rev. Lett. **110**, 112301 (2013).
[8] L. Yan, P. Zhuang, and N. Xu, Phys. Rev. Lett. **97**, 232301 (2006).
[9] Y. Liu, B. Chen, N. Xu, and P. Zhuang, Phys. Lett. B **697**, 32 (2011).
[10] B. Chen, M. Hu, H. Zhang, and J. Zhao, Phys. Lett. B **802**, 135271 (2020).
[11] L. Wen, X. Du, S. Shi, and B. Chen, Chin. Phys. C **46**, 114102 (2022).
[12] L. Wen and B. Chen, Phys. Lett. B **839**, 137774 (2023).
[13] F. Karsch, D. Kharzeev, and H. Satz, Phys. Lett. B **637**, 75 (2006).
[14] H. Satz, J. Phys. G **32**, R25 (2006).
[15] Y. Liu, N. Xu, and P. Zhuang, Phys. Lett. B **724**, 73 (2013).
[16] X. Guo, S. Shi, and P. Zhuang, Phys. Lett. B **718**, 143 (2012).
[17] B. Chen, Y. Liu, K. Zhou, and P. Zhuang, Phys. Lett. B **726**, 725 (2013).
[18] A. Adil and I. Vitev, Phys. Lett. B **649**, 139 (2007).
[19] C. Y. Wong, E. S. Swanson, and T. Barnes, Phys. Rev. C **65**, 014903 (2001); **66**, 029901(E) (2002).
[20] X. l. Zhu, P. f. Zhuang, and N. Xu, Phys. Lett. B **607**, 107 (2005).
[21] X. Du, M. He, and R. Rapp, Phys. Rev. C **96**, 054901 (2017).
[22] J. Zhao and B. Chen, Phys. Lett. B **776**, 17 (2018).
[23] E. Braaten and M. H. Thoma, Phys. Rev. D **44**, R2625 (1991).
[24] M. Gyulassy, P. Levai, and I. Vitev, Phys. Rev. Lett. **85**, 5535 (2000).
[25] M. Djordjevic and M. Gyulassy, Nucl. Phys. A **733**, 265 (2004).
[26] G. Y. Qin, J. Ruppert, C. Gale, S. Jeon, G. D. Moore, and M. G. Mustafa, Phys. Rev. Lett. **100**, 072301 (2008).
[27] U. A. Wiedemann, Nucl. Phys. A **690**, 731 (2001).
[28] N. Armesto, B. Cole, C. Gale, W. A. Horowitz, P. Jacobs, S. Jeon, M. van Leeuwen, A. Majumder, B. Muller, G. Y. Qin *et al.*, Phys. Rev. C **86**, 064904 (2012).
[29] X. f. Guo and X. N. Wang, Phys. Rev. Lett. **85**, 3591 (2000).
[30] A. Majumder and M. Van Leeuwen, Prog. Part. Nucl. Phys. **66**, 41 (2011).
[31] S. A. Bass, C. Gale, A. Majumder, C. Nonaka, G. Y. Qin, T. Renk, and J. Ruppert, Phys. Rev. C **79**, 024901 (2009).
[32] B. Abelev *et al.* (ALICE Collaboration), J. High Energy Phys. 09 (2012) 112.
[33] B. Abelev *et al.* (ALICE Collaboration), Phys. Rev. Lett. **111**, 102301 (2013).
[34] M. He, R. J. Fries, and R. Rapp, Phys. Rev. C **86**, 014903 (2012).
[35] S. Cao, G. Y. Qin, and S. A. Bass, Phys. Rev. C **92**, 024907 (2015).
[36] Y. He, T. Luo, X. N. Wang, and Y. Zhu, Phys. Rev. C **91**, 054908 (2015); **97**, 019902(E) (2018).
[37] X. Yao, W. Ke, Y. Xu, S. A. Bass, and B. Müller, J. High Energy Phys. 01 (2021) 046.
[38] B. Chen, Phys. Rev. C **95**, 034908 (2017).
[39] M. He, B. Wu, and R. Rapp, Phys. Rev. Lett. **128**, 162301 (2022).
[40] X. Du and R. Rapp, Phys. Lett. B **834**, 137414 (2022).
[41] A. H. Mueller and J. w. Qiu, Nucl. Phys. B **268**, 427 (1986).
[42] K. J. Eskola, H. Paukkunen, and C. A. Salgado, J. High Energy Phys. 04 (2009) 065.
[43] K. Zhou, N. Xu, Z. Xu, and P. Zhuang, Phys. Rev. C **89**, 054911 (2014).
[44] D. A. Teaney, *Quark Gluon Plasma 4* (World Scientific, Singapore, 2010).
[45] B. Schenke, S. Jeon, and C. Gale, Phys. Rev. C **82**, 014903 (2010).
[46] C. Shen, U. Heinz, P. Huovinen, and H. Song, Phys. Rev. C **82**, 054904 (2010).
[47] L. Grandchamp, R. Rapp, and G. E. Brown, Phys. Rev. Lett. **92**, 212301 (2004).
[48] X. Du and R. Rapp, Nucl. Phys. A **943**, 147 (2015).
[49] B. Chen, T. Guo, Y. Liu, and P. Zhuang, Phys. Lett. B **765**, 323 (2017).
[50] X. Yao and B. Müller, Phys. Rev. D **100**, 014008 (2019).
[51] X. Yao and T. Mehen, J. High Energy Phys. 02 (2021) 062.
[52] R. L. Thews, M. Schroedter, and J. Rafelski, Phys. Rev. C **63**, 054905 (2001).
[53] B. Chen, L. Jiang, X. H. Liu, Y. Liu, and J. Zhao, Phys. Rev. C **105**, 054901 (2022).
[54] P. Braun-Munzinger and J. Stachel, Phys. Lett. B **490**, 196 (2000).
[55] N. Brambilla, M. Á. Escobedo, M. Strickland, A. Vairo, P. Vander Griend, and J. H. Weber, J. High Energy Phys. 05 (2021) 136.
[56] Y. Akamatsu, M. Asakawa, S. Kajimoto, and A. Rothkopf, J. High Energy Phys. 07 (2018) 029.
[57] X. Yao, Int. J. Mod. Phys. A **36**, 2130010 (2021).
[58] Y. Akamatsu and T. Miura, EPJ Web Conf. **258**, 01006 (2022).
[59] J. P. Blaizot and M. A. Escobedo, Phys. Rev. D **98**, 074007 (2018).
[60] S. Delorme, T. Gousset, R. Katz, and P. B. Gossiaux, Acta Phys. Pol. Supp. **16**, 1-A112.1 (2023).
[61] G. Nijs, B. Scheihing-Hitschfeld, and X. Yao, J. High Energy Phys. 06 (2023) 007.
[62] M. E. Peskin, Nucl. Phys. B **156**, 365 (1979).
[63] G. Bhanot and M. E. Peskin, Nucl. Phys. B **156**, 391 (1979).

[64] B. Chen, Chin. Phys. C **43**, 124101 (2019).
[65] D. Lafferty and A. Rothkopf, Phys. Rev. D **101**, 056010 (2020).
[66] S. Y. F. Liu, M. He, and R. Rapp, Phys. Rev. C **99**, 055201 (2019).
[67] G. Y. Qin, H. Petersen, S. A. Bass, and B. Muller, Phys. Rev. C **82**, 064903 (2010).
[68] M. He, R. J. Fries, and R. Rapp, Phys. Lett. B **735**, 445 (2014).
[69] Y. Xu, J. E. Bernhard, S. A. Bass, M. Nahrgang, and S. Cao, Phys. Rev. C **97**, 014907 (2018).
[70] S. Acharya *et al.* (ALICE Collaboration), Phys. Rev. D **105**, L011103 (2022).
[71] R. Aaij *et al.* (LHCb Collaboration), J. High Energy Phys. 06 (2017) 147.
[72] M. He and R. Rapp, Phys. Rev. Lett. **124**, 042301 (2020).
[73] M. Cacciari, M. Greco, and P. Nason, J. High Energy Phys. 05 (1998) 007.
[74] M. Cacciari, S. Frixione, and P. Nason, J. High Energy Phys. 03 (2001) 006.
[75] R. Rapp, P. B. Gossiaux, A. Andronic, R. Averbeck, S. Masciocchi, A. Beraudo, E. Bratkovskaya, P. Braun-Munzinger, S. Cao, A. Dainese *et al.*, Nucl. Phys. A **979**, 21 (2018).
[76] X. Dong and V. Greco, Prog. Part. Nucl. Phys. **104**, 97 (2019).
[77] M. Yang, S. Zheng, B. Tong, J. Zhao, W. Ouyang, K. Zhou, and B. Chen, Phys. Rev. C **107**, 054917 (2023).
[78] P. A. Zyla *et al.* (Particle Data Group), Rev. Part. Phys. **2020**, 083C01 (2020).
[79] J. Sollfrank, P. Huovinen, M. Kataja, P. V. Ruuskanen, M. Prakash, and R. Venugopalan, Phys. Rev. C **55**, 392 (1997).
[80] W. Zhao, H. j. Xu, and H. Song, Eur. Phys. J. C **77**, 645 (2017).
[81] C. Shen, Z. Qiu, H. Song, J. Bernhard, S. Bass, and U. Heinz, Comput. Phys. Commun. **199**, 61 (2016).
[82] B. Abelev *et al.* (ALICE Collaboration), Phys. Lett. B **718**, 295 (2012); **748**, 472 (2015).
[83] A. M. Sirunyan *et al.* (CMS Collaboration), Phys. Lett. B **790**, 509 (2019).
[84] B. Abelev *et al.* (ALICE Collaboration), J. High Energy Phys. 11 (2012) 065.
[85] D. Acosta *et al.* (CDF Collaboration), Phys. Rev. D **71**, 032001 (2005).
[86] V. Khachatryan *et al.* (CMS Collaboration), Eur. Phys. J. C **71**, 1575 (2011).
[87] J. W. Cronin *et al.* (E100 Collaboration), Phys. Rev. D **11**, 3105 (1975).
[88] X. Bai (ALICE Collaboration), EPJ Web Conf. **276**, 02015 (2023).
[89] S. Acharya *et al.* (ALICE Collaboration), Phys. Rev. Lett. **119**, 242301 (2017).
[90] S. Acharya *et al.* (ALICE Collaboration), J. High Energy Phys. 10 (2020) 141.